Langmuir

Article

pubs.acs.org/Langmuir

Grazing-Incidence Neutron-Induced Fluorescence Probes Density Profiles of Labeled Molecules at Solid/Liquid Interfaces

Emanuel Schneck,*[,†,‡] Michael Jentschel,[‡] Christian Gege,[†] Motomu Tanaka,[†] and Bruno Demé*[,‡]

[†]Physical Chemistry of Biosystems, Institute of Physical Chemistry, University of Heidelberg, D-69120 Heidelberg, Germany

[‡]Institut Laue-Langevin, 6 rue Jules Horowitz, F-38042 Grenoble Cedex 9, France

Supporting Information

ABSTRACT: We report on the use of characteristic prompt γ-fluorescence after neutron capture induced by an evanescent neutron wave to probe densities and depth profiles of labeled molecules at solid/liquid interfaces. In contrast to classical scattering techniques and X-ray fluorescence, this method of "grazing-incidence neutron-induced fluorescence" combines direct chemical specificity, provided by the label, with sensitivity to the interface, inherent to the evanescent wave. We demonstrate that the formation of a supported lipid membrane can be quantitatively monitored from the characteristic fluorescence of $^{157}Gd^{3+}$ ions bound to the headgroup of chelator lipids. Moreover, we were able to localize the $^{157}Gd^{3+}$ ions along the surface normal with nanometer precision. This first proof of principle with a well-defined model system suggests that the method has a great potential for biology and soft matter studies where spatial resolution and chemical sensitivity are required.

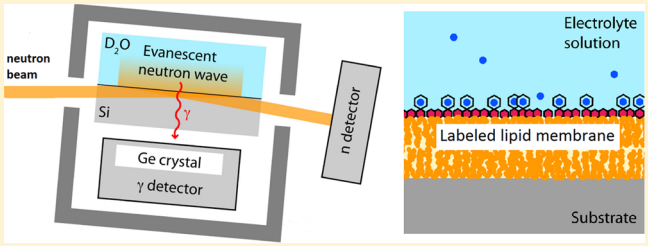

I. INTRODUCTION

Lipid membranes deposited on planar substrates[1,2] have been commonly used as model systems of biomembranes. Single supported membranes or multilayers[3] are versatile platforms for the study of biological surfaces and can be investigated in various aspects including membrane structure, mechanics, dynamics, and molecular interactions. X-ray and neutron scattering provide spatial resolution at molecular length scales and access to buried structures and become especially powerful when samples possess planar geometry, allowing the simultaneous probing of structures perpendicular and parallel to the surface. Using this approach, various properties of biomembranes have been studied, which include structural aspects,[4−9] dynamics of lipid molecules,[10,11] and membrane mechanics.[4,8,12−14] While grazing-incidence small-angle scattering (GISAXS and GISANS) yields information on in-plane structures close to the surface,[15−17] reflectometry is a powerful scattering technique to determine density profiles perpendicular to the surface.[4,6,9,18] However, despite the development of isotopic substitution,[5] classical scattering techniques are intrinsically lacking direct chemical sensitivity. This becomes problematic in cases of soft and complex interfaces with graded scattering length density (SLD) profiles, where the distributions of different molecules cannot be determined unambiguously. Sensitivity to chemical elements is provided by grazing-incidence X-ray fluorescence (GIXF), which utilizes an evanescent X-ray wave at the air/water interface to probe density profiles of chemical elements by inducing characteristic fluorescence.[19,20] This method revealed ion distributions at the air/water interface[21,22] but cannot be transferred to solid/liquid interfaces. As an alternative, standing-wave X-ray fluorescence (SWXF) has been employed to study elemental distributions near solid surfaces,[23−26] but since the beam is transmitted through the aqueous phase, fluorescence background is generated unless the bulk concentrations of target elements are very low. In summary, a technique to probe solid/liquid interfaces that combines direct chemical specificity with inherent sensitivity to the interface would be desirable in colloidal chemistry, biochemistry, and material science. Here, we introduce grazing-incidence neutron-induced fluorescence (GINF), a method to probe the interfacial density of labeled molecules at solid/liquid interfaces with an evanescent neutron wave. The method is based on the prompt emission of γ radiation after neutron capture, a principle that has been successfully applied by Zhang et al. to study thin solid films in neutron standing-wave experiments.[27,28] But despite medical applications for the detection of chemical elements in tissues,[29,30] neutron-induced γ radiation has so far not been used to probe dilute layers of labeled molecules in aqueous environments. GINF utilizes an evanescent neutron wave near a solid/liquid interface to induce the characteristic γ-fluorescence of the nuclide label. The technique is applicable to all systems where nuclides that possess high cross sections for neutron capture—such as ^{157}Gd, ^{149}Sm, ^{113}Cd, and ^{10}B—can be used as labels. It has therefore a great potential in colloidal chemistry, biochemistry, and material science. In the present study, a supported membrane incorporating chelator lipids that complex Gd^{3+} ions is investigated. The membrane is

Received: January 14, 2013
Revised: February 27, 2013
Published: March 5, 2013

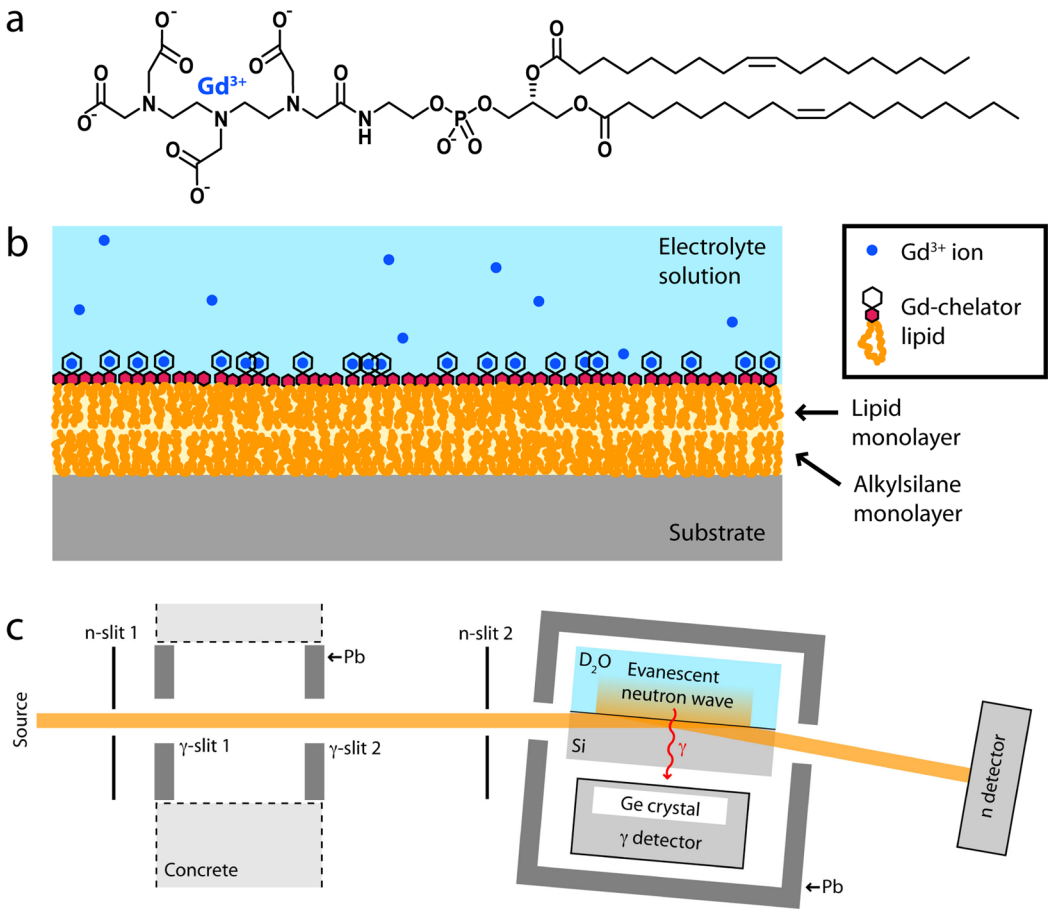

Figure 1. (a) Chemical structure of the Gd–chelator lipid forming a complex with a Gd^{3+} ion. (b) Illustration of the solid-supported lipid membrane. The membrane consists of a substrate-grafted alkylsilane monolayer, on top of which a lipid monolayer is deposited by fusion of unilamellar vesicles. The monolayer contains defined amounts of Gd–chelator lipid. (c) Setup for grazing-incidence neutron-induced fluorescence experiments at the solid/liquid interface. An evanescent neutron wave created in the liquid phase near the interface induces γ-fluorescence via neutron capture by nuclide labels. The characteristic fluorescence γ radiation is recorded with an energy-sensitive γ-detector.

formed by fusion of unilamellar vesicles on a monolayer of alkyl chains grafted onto the silicon surface.[9,31] We demonstrate that GINF can quantify the surface density of the ^{157}Gd label bound to the membrane surface and that it can localize it with nanometer precision.

II. EXPERIMENTAL DETAILS AND METHODS

A. Chemicals and Sample Preparation. Unless stated otherwise, all chemicals were purchased from Fluka (Taufkirchen, Germany) and used without further purification. D_2O was purchased from Eurisо-Top, Saint-Aubin, France. $GdCl_3$ was prepared from Gd_2O_3 by addition of concentrated HCl solution and subsequent drying in a rotary evaporator. The Gd_2O_3 was 91% enriched in its ^{157}Gd content (f_{157} = 0.91) and purchased from Trace Science International, Richmond Hill, Canada. In order to remove remaining traces of H_2O, the resulting $GdCl_3$ salt was redissolved in D_2O several times and dried again. In the last step, D_2O was added to generate a 30 mM $GdCl_3$ stock solution, which was diluted with D_2O-based electrolyte solutions. 1-Stearyl-2-oleoyl-*sn*-glycerophosphatidylcholine (SOPC) was purchased from Avanti Polar Lipids (Alabaster, AL). The Gd–chelator lipid was prepared by reaction of 1,2-dioleoyl-*sn*-glycero-3-phosphoethanolamine (Sigma) with diethylenediaminepentaacetic acid dianhydride (Aldrich) as previously described for the dipalmitoyl analogue.[32] Figure 1a shows the Gd–chelator lipid in its fully deprotonated state forming a complex with a Gd^{3+} ion. Vesicle suspensions were prepared by mixing chloroform solutions of SOPC and Gd–chelator lipid in defined quantities. The dry lipid mixtures were then suspended into D_2O-based electrolyte solutions at a concentration of 5 mg/mL, incubated for 6 h at 40 °C, and tip-sonicated in order to create small unilamellar vesicles (SUVs). Subsequently, the SUV suspensions were diluted to a final concentration of 0.5 mg/mL in electrolyte solutions containing 100 mM NaCl and $GdCl_3$ at defined concentrations. For GINF measurements two different types of monocrystalline silicon (100) blocks (Holm Silicon, Tann, Germany) were used, with a topological root-mean-square (rms) roughness of ≈0.5 nm and dimensions of either 80 × 50 × 15 mm^3 or 100 × 60 × 5 mm^3. The silicon chips used for X-ray reflectometry (Si-Mat, Landsberg/Lech, Germany) had identical specifications and dimensions of 24 × 10 × 0.65 mm^3. All silicon surfaces were rendered hydrophobic with a monolayer of octadecylsilane covalently grafted to the native silicon oxide to form a homogeneous monolayer of alkyl chains.[33] The samples were then inserted into liquid cells and exposed to H_2O-based (X-ray measurements) or D_2O-based (neutron measurements) electrolyte solutions containing 100 mM NaCl and $GdCl_3$ at defined concentrations. For the formation of the lipid membranes, SUV suspensions containing 40 mol % (f_{ch} = 0.4) Gd–chelator lipid were injected into the liquid cells and incubated for >1 h in contact with the hydrophobic surface. The hydrophobic alkylsilane monolayer triggers the fusion of vesicles and the formation of a lipid membrane.[9] At room temperature, SOPC is in the fluid phase, with an average area per lipid molecule of $A \approx 0.61$ nm^2 (see ref 34), and it has been demonstrated that hybrid bilayers consisting of a surface-grafted alkylsilane layer and a lipid monolayer behave as two structurally uncoupled monolayers.[35,36] The architecture of the solid-supported lipid membranes is illustrated in Figure 1b. Mixtures of phospholipids and lipid-anchored chelators have also been studied by other groups.[37,38]

dx.doi.org/10.1021/la400162y | *Langmuir* 2013, 29, 4084–4091

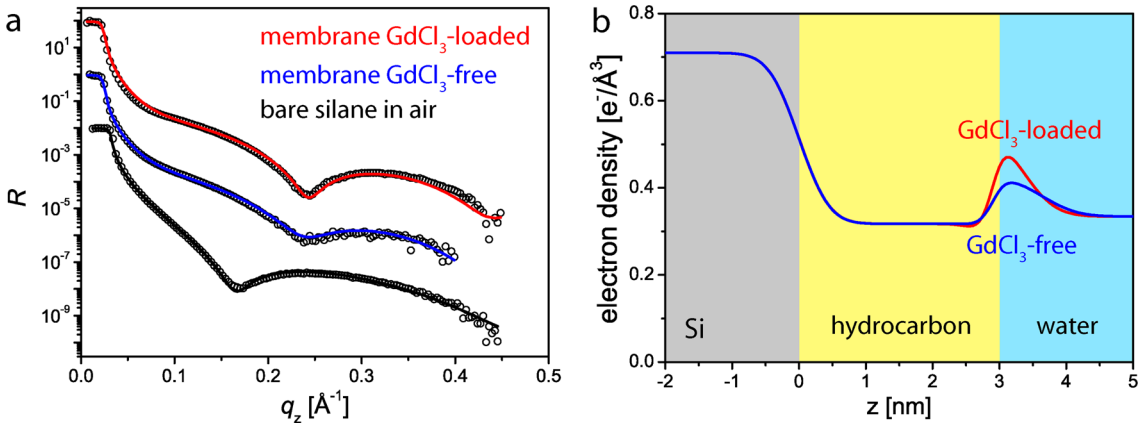

Figure 2. (a) X-ray reflectivity of the silane-functionalized silicon substrate in air (bottom), after the formation of a SOPC monolayer incorporating 40 mol % chelator lipid in $GdCl_3$-free buffer (middle), and after rinsing with a buffer containing 200 μM $GdCl_3$ (top). Curves are shifted vertically for clarity. Open symbols represent experimental data. Solid lines represent calculated reflectivities based on a slab-model representation of the interfacial electron density profiles. (b) Reconstructed electron density profiles for supported membranes in buffer with and without $GdCl_3$. Model parameters for the membrane in $GdCl_3$-loaded buffer are summarized in Table 1.

B. Experimental Setup and Measurements. GINF experiments were carried out at the D16 diffractometer of the Institut Laue-Langevin (ILL, Grenoble, France). The experimental setup (top view) is illustrated in Figure 1c. In the GINF experiments a vertically focused monochromatic neutron beam with $\lambda = 4.72$ Å and $\Delta\lambda/\lambda = 1\%$ reaches the interface between the silicon substrate and the D_2O-based aqueous solution through the silicon substrate. The critical angle of total reflection in this configuration is $\theta_c = 0.316°$. The angular divergence of the neutron beam in the plane of incidence was about $\delta\theta = 0.01°$, as defined by the widths of the slits (n-slit 1 and n-slit 2) and by the slit distance. Neutrons are captured by the $^{157}Gd^{3+}$ ions bound to the membrane surface. At $\lambda = 4.72$ Å, the neutron capture cross section of ^{157}Gd is as large as $\sigma = 0.53$ Mb[39] (megabarns). After capture, the resulting ^{158}Gd nuclide is in an excited state that promptly decays to the ground state through various channels. The strongest line is at 182 keV with a yield of $\phi_{182} = 0.183$ photons per neutron capture.[39] The 182 keV photons are transmitted through the silicon substrate and detected with an energy-sensitive γ-detector. The nuclear reaction employed for the measurement can be summarized as [^{157}Gd + n → ^{158}Gd + $\gamma_{182\ keV}$ + other γs]. The 182 keV photons emitted after neutron capture are detected with a high-purity germanium detector (Coaxial HPGe, 3 in. diameter, 25% relative efficiency, Canberra Industries, Meriden) cooled with liquid N_2. In order to minimize the background, a dedicated shielding for sample environment and γ-detector was designed as well as an additional γ-collimator consisting of two pairs of lead slits placed at the exit of the monochromator casemate.

The angle-dependent fluorescence intensity (i.e., the γ count rate) $r(\theta_i)$ is proportional to the spatial integral over the product of the label density profile $\rho(z)$ and the angle dependent neutron density profile $I(\theta_i z)$:

$$r(\theta_i) = B(\theta_i)\int_{-\infty}^{\infty} I(\theta_i, z)\rho(z)\,dz \tag{1}$$

This is in full analogy to the case of X-rays[20−22] when the depth dependence of fluorescence reabsorption is neglected. The angle-dependent prefactor B is determined by the beam footprint, by the (weak) angle dependence of the γ detection efficiency, and by a number of angle-independent setup parameters (see further below). $I(\theta_i z)$ was computed from a suitable slab model representation of the interfacial SLD profile (see below) by a phase-correct summation of all reflected and transmitted partial waves as has been described previously for X-rays[19,22] and neutrons[27,28,40] (see also Supporting Information). In this calculation, interfacial roughness was rightfully neglected, since the corresponding Névot−Croce factors $\exp(-(q_z\sigma)^2/2)$ are close to unity in the considered angle range, where $q_z = 4\pi \sin\theta_i/\lambda$.

X-ray reflectivity curves were measured using a Bruker D8 Discover X-ray reflectometer with molybdenum anode and 17.5 keV beam energy.

C. Prediction of Absolute γ Count Rates. For a fixed incident angle θ_i, the absolute rate r with which the detection system counts 182 keV photons emitted by the labeled membrane surface can be expressed as

$$r = Q_n P_c P_d \tag{2}$$

where $Q_n = 1480 \pm 20\ s^{-1}$ denotes the incident neutron flux, P_c the probability of each incident neutron to be captured by ^{157}Gd bound to the membrane surface, and P_d the probability of each capture event to be recognized by the setup via detection of a 182 keV photon. Note that the low neutron flux results from the narrow slit at the sample (n-slit 2, closed to 150 micrometers horizontally) required for sample under-illumination below the critical angle of total reflection.

For a sharp (delta-like) ^{157}Gd distribution at the membrane surface, P_c can be expressed in terms of the average transmittivity $\langle T_n\rangle \approx 0.91$ of the silicon substrate for the incident neutrons, the ratio between capture cross-section σ and average area A^* per surface-bound ^{157}Gd normal to the beam, and the relative neutron density at the membrane surface I_{surf}/I_0 with respect to the incident beam.

$$P_c = \langle T_n\rangle \frac{\sigma}{A^*}\frac{I_{surf}}{I_0} \tag{3}$$

A^*, in turn, follows from f_{ch}, f_{157}, and θ_i (see above), from the membrane area per lipid molecule A, and from the average number n_{ch} of Gd^{3+} ions associated with one Gd−chelator lipid:

$$A^* = \frac{A}{f_{ch} f_{157} n_{ch}} \sin\theta_i \tag{4}$$

For $\theta_i = 0.28°$, the neutron density at the membrane surface, I_{surf}, is more than 3 times higher than in the incident beam ($I_{surf}/I_0 = 3.3 \pm 0.3$, see Figure 4a). This value is robust with respect to variations in the slab representation of the hydrocarbon layer. The error associated with I_{surf}/I_0 mainly represents the uncertainty in the exact z-location of the Gd^{3+} ions at the membrane surface ($\delta z \approx 1$ nm).

P_d in eq 2 is characterized by the fluorescence yield ϕ_{182}, by the transmittivity $T_\gamma \approx 0.65$ of the silicon substrate for 182 keV photons,[41] and by the counting efficiency $\eta_\gamma = 0.050 \pm 0.005$ of the detection system for 182 keV photons in the measurement configuration, which was thoroughly measured by exposure of a calibration standard of known neutron conversion efficiency with the collimated incident beam at the sample position:

$$P_d = \phi_{182}\eta_\gamma T_\gamma \tag{5}$$

dx.doi.org/10.1021/la400162y | Langmuir 2013, 29, 4084−4091

Besides n_{ch}, all parameters are known with reasonable accuracy, so that r can be rewritten as

$$r = \alpha n_{ch} \quad (6)$$

where $\alpha = 0.18 \pm 0.05\ s^{-1}$. The relative uncertainty in α ($\alpha\Delta/\alpha \approx 0.3$) mainly results from the relative uncertainties in A, I_{surf}/I_0, and η_γ (all ≈0.1), but to a lesser extent also from the relative uncertainties in the other parameters (between 0.02 and 0.05).

III. RESULTS AND DISCUSSION

Figure 1b schematically shows the sample architecture after formation of a solid-supported lipid membrane by vesicle fusion. The sample structure is first characterized by high-energy X-ray reflectometry. Figure 2a shows X-ray reflectivity curves of the bare silane-functionalized silicon substrate in air (bottom), after membrane formation in $GdCl_3$-free buffer (middle), and after rinsing with a buffer containing 200 μM $GdCl_3$ at pH 6 (top). Note that the same sample was used for all three reflectivity measurements and that surface modifications were performed in situ between the acquisitions. Open symbols represent experimental data. Solid lines represent calculated reflectivities based on a slab-model representation of the interfacial electron density profiles. For the description of the bare silane-functionalized substrate, a one-slab-model was used, representing the hydrocarbon layer between silicon and air bulk media. For the description of the supported membrane in water, a two-slab-model was employed, with one slab representing the hydrocarbon layer jointly formed by silane and lipid alkyl chains and one slab representing the lipid headgroups of SOPC and chelator lipid. The best-matching model parameters of the membrane in $GdCl_3$-loaded buffer (electron densities ρ_e of slabs and bulk media, slab thicknesses d, and root-mean-square roughness parameters σ of the interfaces) are summarized in Table 1. The parameters for the other conditions are given in the Supporting Information. In order to minimize the number of independent fitting parameters, all three curves were fitted simultaneously, with common parameters for the roughness of the interface between silicon substrate and hydrocarbon layer and for the electron density of the hydrocarbon layer. Figure 2b shows the reconstructed electron density profiles of supported membranes in $GdCl_3$-free (blue line) and $GdCl_3$-loaded (red line) buffer. The membrane jointly formed by the alkyl chains of silane and lipid monolayer can be represented with a slab of about 3 nm thickness at the interface between silicon and water. The significant increase in the headgroup electron density in the presence of $GdCl_3$ can be attributed to the binding of Gd^{3+} ions to the negatively charged chelator lipids incorporated in the membrane. We find that the ions are confined close to the membrane surface, at a distance of below about 1 nm from the hydrocarbon layer. The z-integrated electron density difference between $GdCl_3$-free and $GdCl_3$-loaded cases corresponds to an area excess of 0.24 $e^-/Å^2$, reasonably close to the estimated value of 0.34 $e^-/Å^2$, which assumes the displacement of 3 Na^+ ions (corresponding to 30 electrons) by each Gd^{3+} ion (corresponding to 61 electrons) and a membrane area of 90 $Å^2$ per Gd^{3+} ion. The latter number is estimated from the area per lipid molecule (≈60 $Å^2$), the density of chelator lipids (40 mol %), and from the maximal charge per chelator lipid (−5 e^-). The actual Gd density at the interface, however, is difficult to quantify by our X-ray reflectivity measurements alone, since differences in ionic volumes as well as the displacement of water molecules and molecular rearrangements induced by the presence of $GdCl_3$ contribute to changes in the interfacial electron density profile.

Table 1. Membrane Electron Density Model Parameters in the Presence of $GdCl_3$[a]

	silicon	hydrocarbon	headgroup	water
ρ_e ($e^-/Å^3$)	0.71	0.32	0.56	0.33
d (Å)	∞	29	4	∞
σ (Å)	4	2	4	

[a] ρ_e denotes the electron density, d the thickness, and σ the rms roughness of each slab with the adjacent medium.

In the present study the Gd density at the membrane surface is high enough to deduce the label position from the X-ray reflectivity measurements, which provides us with an independent validation of the GINF results detailed further below. We would like to point out, however, that when dealing with more complex soft interfaces (i.e., with lower label densities and more diffuse label distributions) or lighter labels, this would become hardly feasible. In these cases it will be more rewarding to determine SLD profiles by neutron reflectivity measurements in parallel with GINF.

During GINF measurements the neutron beam impinges onto the silicon/D_2O interface at an incident angle θ_i below or slightly above the critical angle of total reflection $\theta_c = 0.316°$. For illumination below θ_c, the lipid membrane at the interface is illuminated with an evanescent neutron wave with a decay length in the nanometer range. Because of interference of incident and reflected neutron beams, the neutron density at the membrane surface in general deviates substantially from that of the incident beam, depending on θ_i (see Figure 4a). The inset of Figure 3a shows the neutron reflectivity curve (symbols with error bars) of a sample around the critical angle of total reflection. All features characterizing the sample alignment coincide with the geometrical prediction (indicated with a solid red line), including the transition from over- to under-illumination at $\theta_i \approx 0.13°$, the flat plateau of total reflection, and the position of the critical angle of total reflection, $\theta_c \approx 0.32°$. The intensity of the reflected beam in the plateau is slightly lower than that of the incident beam, depending on the amount of diffuse scattering from the topologically rough interface and on the level of neutron absorption. It has been shown that the intensity loss below the critical angle can be analyzed to deduce the composition of porous thin films.[42] In the absence of $GdCl_3$ (without neutron absorption by the ^{157}Gd label) the decrease is still significant (≈4%). The amount of diffuse scattering depends on the topological roughness of the interface. Quantifying the neutron capture rate from a decrease in specular reflectivity alone is therefore not possible without an independent measurement of the total diffuse intensity. In our measurements, in contrast, the capture rate by the label is unambiguously measured from the intensity of the characteristic lines in the γ-spectrum. Importantly, the relative statistical error of a GINF experiment is lower than that of the corresponding reflectometry experiment when neutron absorption is weak (see Supporting Information).

In a first set of experiments, GINF measurements were carried out at a fixed angle of incidence of $\theta_i = 0.28°$, well within the plateau of total reflection (see inset Figure 3a). The relative energy resolution of the γ-spectra at 182 keV was about 2%. The spectra recorded before (dotted black line) and after (solid red line) the formation of the ^{157}Gd-labeled membrane at the interface are presented in the main panel of Figure 3a. In both cases the aqueous electrolyte solution contains 200 μM

dx.doi.org/10.1021/la400162y | Langmuir 2013, 29, 4084−4091

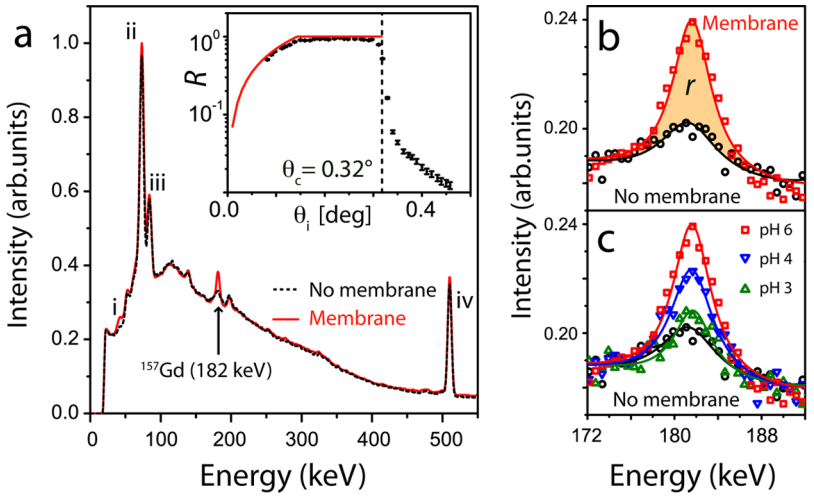

Figure 3. (a) γ-Spectra recorded before (black) and after (red) the formation of a Gd-labeled membrane at the interface. The characteristic fluorescence at 182 keV after neutron capture by ^{157}Gd is indicated with an arrow. Characteristic energies of internal conversion, Pb Kα, Pb Kβ, and pair annihilation are denoted i, ii, iii, and iv, respectively (see main text). The inset shows the neutron reflectivity curve around the critical angle of total reflection of an aligned sample. Error bars represent the statistical error of the neutron counting. The critical angle θ_c is indicated with a dotted vertical line. Solid red lines superimposed on the data points represent the predicted curve at low incident angles. (b) Intensity of the 182 keV line before (black) and after (red) the membrane formation. The area between the two peaks (shaded in orange) corresponds to the count rate r. (c) 182 keV line intensity subject to variations in the bulk pH, reflecting the pH dependence of the chelator binding efficiency.

$GdCl_3$ at pH 6. The spectra exhibit a clear difference in the characteristic 182 keV line emitted after neutron capture by ^{157}Gd. Another characteristic feature is observed at 43 keV, resulting from internal conversion of Gd after neutron capture[43] (see also Supporting Information). The second strongest line of the ^{157}Gd neutron capture reaction at 79 keV (see Supporting Information) is hidden between the Kα and Kβ lines of Pb and therefore difficult to observe. The peak at 511 keV originates from the ubiquitous electron/positron pair annihilation. Figure 3b shows the 182 keV peak obtained before and after formation of the Gd-labeled membrane (symbols) together with the best Lorentzian fits (solid lines). The neutron capture signal is strongly increased by the formation of the Gd-labeled membrane at the interface (red line). It should be noted that significant 182 keV intensity is found even before fusion of vesicles (black) when ^{157}Gd is already present in the subphase. However, its bulk concentration (200 μM) is too low to explain this signal from the bulk-level abundance of ^{157}Gd in the first few nanometers probed by the evanescent neutron wave. Instead, the signal has to be attributed to neutrons that are scattered into the aqueous volume and captured by ^{157}Gd. This signal before the formation of the membrane is therefore the correct reference to consider (in the absence of ^{157}Gd in the bulk no signal is detected at 182 keV). The absolute count rate originating from ^{157}Gd bound to the membrane surface at 182 keV, r, is thus the difference between the integrated intensities (i.e., areas under the peaks) before and after the formation of the membrane. The count rate can be related quantitatively to the number n_{ch} of Gd^{3+} ions associated with one Gd-chelator lipid: $r = \alpha n_{ch}$, where $\alpha = 0.18 \pm 0.05$ s^{-1} (see Experimental Details and Methods). We find that $r \approx 0.32$ s^{-1}, corresponding to $n_{ch} = 1.8 \pm 0.5$. This result appears reasonable, as each Gd–chelator lipid can possess up to five negative charges at neutral pH, located at one phosphate group and four carboxyl groups (see Figure 1a). The charges remaining after complexation of one Gd^{3+} have to be screened by the electrolyte. This screening is largely dominated by the trivalent Gd^{3+} ions, such that up to $n_{ch} = 5/3 \approx 1.67$ is expected. In summary, we find remarkable agreement between estimated and measured fluorescence intensities.

In the same set of experiments we explored the pH dependence of n_{ch}, which reflects the pH dependence of the complexation efficiency between Gd^{3+} and the Gd–chelator lipids. For that purpose the liquid cell was rinsed with an excess of aqueous electrolyte of the same composition, but at different pH values. Figure 3c shows the 182 keV line intensity for various pH values. A clear trend is observed: the count rate originating from the membrane decreases with decreasing pH. Starting from $r \approx 0.32$ s^{-1} at pH 6, the count rate decreases to $r \approx 0.19$ s^{-1} at pH 4, corresponding to $n_{ch} = 1.1 \pm 0.3$. At pH 3, r becomes almost insignificant. The observed trend can be understood from the pK values of the carboxyl groups in the Gd–chelator lipids, which lose their negative charge at low pH via protonation. As a consequence, the complexation efficiency decreases with decreasing pH. The result is in good qualitative agreement with titration curves of DTPA–lanthanide complexes,[44] whose charge is pH sensitive mostly in the interval ($2.5 < \text{pH} < 4.5$). For our system the interval is shifted to slightly higher values (we find a clear difference between pH 6 and pH 4; see Figure 3c), which indicates that Gd^{3+} is more easily released from the chelator lipid than from free DTPA. This can be attributed to the fact that, in the chelator lipid, one carboxyl group of DTPA is involved in the binding to the lipid anchor (see Figure 1a) and can, thus, not contribute to complex formation. It has been shown that the number of carboxyl groups has a significant influence on the complexation strength.[45] The electrostatics at charged interfaces in the presence of multivalent ions is a complex problem in general, due to ion-correlation effects[46] influencing the local pH near the charged surface and due to the fact that pK values at an interface can differ from those of isolated groups in bulk.[47] Theory can thus profit strongly from direct measurements of interfacial ion distributions as presented here and in previous studies.[16]

According to eq 1, the fluorescence intensity emitted by the sample is proportional to the neutron density at the label

dx.doi.org/10.1021/la400162y | Langmuir 2013, 29, 4084–4091

position, which depends on the incident angle θ_i and on the interfacial scattering length density (SLD) profile. In a simple slab model of the SLD profile, the membrane formed by the hydrogenated alkyl chains of silane and the phospholipid monolayers can be represented with one slab of low SLD ($\approx -0.5 \times 10^{-6}$ Å^{-2}) and a thickness of about 3 nm (as determined by X-ray reflectometry, see Table 1) at the interface between silicon (SLD: 2.07×10^{-6} Å^{-2}) and D_2O (SLD: 6.37×10^{-6} Å^{-2}). This is shown in Figure 4a (black line), together

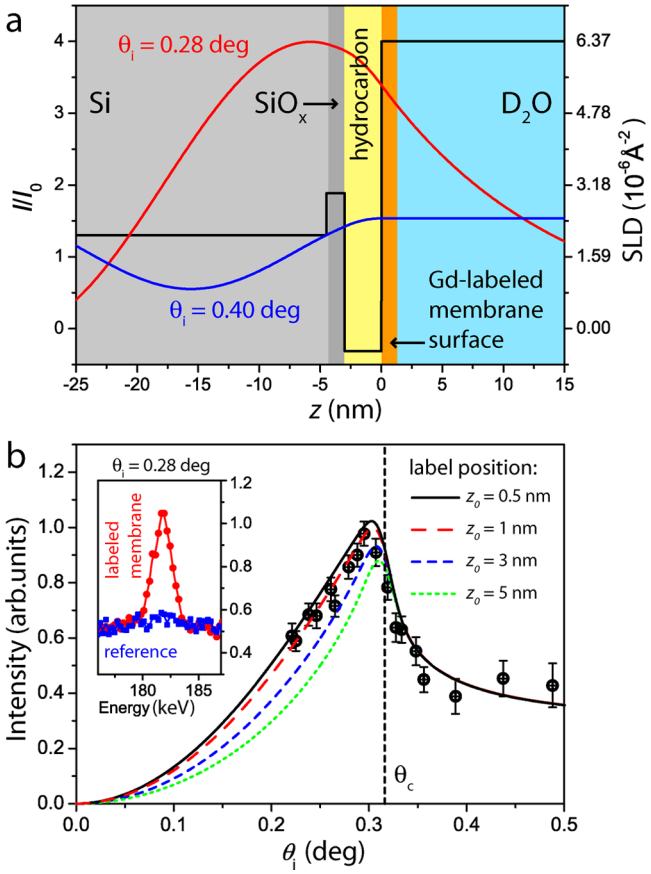

Figure 4. (a) Slab model (black line associated with the right axis) of the scattering length density (SLD) profile around the solid/liquid interface accommodating the ^{157}Gd-labeled lipid membrane and corresponding neutron density profiles (red and blue lines associated with the left axis) computed for the $\theta_i = 0.28° < \theta_c$ (red) and $\theta_i = 0.40° > \theta_c$ (blue). Because of interference the neutron density at the labeled membrane surface deviates from that of the incident beam, I_0. $z = 0$ denotes the interface between alkyl chains and the aqueous region including hydrated lipid headgroups. (b) Normalized fluorescence intensity from the labeled membrane (symbols with error bars) after reference subtraction as a function of θ_i. Error bars represent standard errors of the fluorescence intensity. Lines are theoretical predictions for various positions z_0 of the ^{157}Gd labels. Inset: γ spectra around 182 keV of labeled membrane (red) and reference system (blue) measured for $\theta_i = 0.28°$.

with interfacial neutron density profiles calculated according to this slab model for $\theta_i = 0.28°$ (red line) and $\theta_i = 0.40°$ (blue line) as described in the Experimental Details and Methods. Accounting for the thin oxide layer (SiO_x) at the substrate surface has no significant influence. In a second set of experiments with further optimized sample geometry and improved detection resolution (about 1% relative energy resolution, see Supporting Information) we used the θ_i dependence of the interfacial neutron density to spatially localize the ^{157}Gd labels at the membrane surface. For this purpose, θ_i was varied around the critical angle of total reflection, and the characteristic fluorescence intensity from a ^{157}Gd-labeled membrane surface was recorded. In order to be sensitive solely to the membrane-bound ^{157}Gd, we kept the bulk concentration of $GdCl_3$ as low as 5 μM and subtracted the weak reference signal generated at the same bulk concentration by a membrane without Gd−chelator lipids. The inset of Figure 4b shows γ spectra around 182 keV of labeled membrane and reference system for $\theta_i = 0.28°$. The main panel of Figure 4b shows the corrected fluorescence intensity as a function of θ_i. Data points are normalized to the size of the beam footprint, to the incoming neutron flux, and to the θ_i dependence of the fluorescence detection efficiency (determined independently with the same geometry). Error bars indicate the standard error of the fitted 182 keV peak intensity in the γ spectra. Incident angles below 0.20° are not considered in order to strictly ensure sample under-illumination. The angle dependence of the fluorescence signal contains accurate information on the z-distribution of the label. The lines superimposed on the data points represent theoretical predictions of the intensities, based on the interfacial SLD profile and on the position of the ^{157}Gd labels. The modeled intensities account by convolution for the finite angular divergence of the incident neutron beam ($\delta\theta = 0.01°$, see Experimental Details and Methods) and are scaled to match experimental data points at large angles (above θ_c), where the neutron density in the aqueous medium is z-independent and intensities are, thus, not depending on the label distribution. Label distributions were modeled as sharp Gaussian peaks (fwhm = 0.5 nm = 2.355σ) in the aqueous medium in a distance z_0 from the interface with the hydrocarbon layer:

$$\rho(z) \propto \exp(-(z - z_0)^2/2\sigma^2) \quad (7)$$

Solid black and dashed red lines in Figure 4b correspond to $z_0 = 0.5$ nm and $z_0 = 1$ nm, respectively. Both are plausible assumptions considering the extension of the Gd−chelator lipid headgroups at the membrane surface. The dashed blue line corresponds to $z_0 = 3$ nm, which is unlikely from a structural viewpoint (see X-ray reflectometry results, Figure 2b), and the dotted green line to $z_0 = 5$ nm, which is physically nonrealistic. Clearly, only the first two models ($z_0 \leq 1$ nm) are in agreement with the measured data points within the error, while the other two scenarios can be excluded. This result demonstrates that GINF has the potential to localize labeled molecules at solid/liquid interfaces with nanometer precision. It should be noted, though, that the resolution with which general molecular distributions of unknown shape can be determined has yet to be explored.

In the present study the label density was chosen to be very high (40 mol % Gd−chelator lipid), for a first proof of principle. The enrichment of heavy Gd^{3+} ions at the membrane surface can even be resolved (albeit not quantified unambiguously) by classical X-ray reflectometry (see above). We would like to point out, however, that GINF does not require heavy target elements in general. The label boron (B), for instance, is very light and more generally applicable from a chemical viewpoint, as it is accessible to covalent chemistry.[48] The labels suitable for GINF are not commonly used in biology and soft matter, but when employed at sufficiently low concentrations and bound to chelators, also the multivalent

dx.doi.org/10.1021/la400162y | Langmuir 2013, 29, 4084−4091

ions Gd^{3+}, Cd^{2+}, and Sm^{3+} do not necessarily perturb the studied system more than do popular label types such as heavy metals or chromophores. In fact, chelated Gd^{3+} is widely used as a contrast agent in *in vivo* MRI diagnostics.

Nevertheless, GINF will hardly be able to compete with reflectometry in its classical domain. For the study of well-structured interfaces with dense molecular layers, X-ray and neutron reflectometry with contrast variation or selective deuteration achieve unmatched spatial resolution.[49,50] The application area of GINF we therefore expect to be mostly where classical reflectometry at the solid/liquid interface reaches its limits. GINF may be the method of choice when molecular distributions of interest are too dilute or too diffuse to provide sufficient SLD contrast for classical reflectometry. Applications may include studies of (i) the orientation of end-labeled macromolecules at interfaces or the end point distribution of polymer chains, (ii) distributions of biomolecules interacting weakly with diffuse interfaces, (iii) interfacial depletion effects (e.g., the exclusion of peptides or proteins from crowded layers or extracellular matrices), (iv) the permeation kinetics of labeled molecules through pores or defects in supported membranes, or (v) the diffusion kinetics of biomolecules through gels or crowded layers. The unique isotopic sensitivity may be exploited for studies on the lifetime of ion−chelator complexes and its dependence on pH and ion concentration. We estimate that the current GINF setup provides sufficient signal/noise ratio to work with label densities of one label per 10 nm^2. Further optimization of detection efficiency and the use of time-of-flight measurements may lead to an additional gain in sensitivity of 1 order of magnitude.

IV. CONCLUSIONS

The combination of chemical (and isotopic) specificity with inherent sensitivity to the interface and depth resolution in the nanometer range makes GINF a unique method for the study of planar solid/liquid interfaces in a nondestructive way. These advantages are only achieved with neutrons, which, in contrast to other types of radiation, can form an evanescent wave in the liquid phase with a decay length of several nanometers. The technique can be applied in situ during classical neutron reflectivity experiments, allowing for the simultaneous determination of global density profiles and specific atomic or molecular distributions. GINF has therefore a great potential in colloidal chemistry, biology, and material science.

■ ASSOCIATED CONTENT

Supporting Information

An explicit description of the calculation of neutron density profiles, a sensitivity comparison of reflectivity and GINF to absorption, additional X-ray reflectometry results, and details on the γ detection with improved energy resolution. This material is available free of charge via the Internet at http://pubs.acs.org.

■ AUTHOR INFORMATION

Corresponding Author

*E-mail: schnecke@ill.fr (E.S.), deme@ill.fr (B.D.).

Notes

The authors declare no competing financial interest.

■ ACKNOWLEDGMENTS

We thank the ILL for neutron beamtime on the D16 instrument and for funding the project. Luc Didier and the ILL design office are gratefully acknowledged for the design of γ-shielding and γ-collimation and for technical support. We thank Roman Gernhäuser, Robert Cubitt, Giovanna Fragneto, and Jean Daillant for insightful comments, Alexandra Burk, Nataliya Frenkel, and Viktoria Ganza for help with sample preparation and characterization, Engineering Office Kirchhoff for technical support during the initial stage of the project, and Dan Kirschner and Peter Timmins for carefully reading the manuscript. The work was funded by the ILL and by the Enable Fund of Heidelberg University within the framework of German Excellence Initiatives. E.S. was supported by a Marie Curie Fellowship.

■ REFERENCES

(1) Sackmann, E. Supported Membranes: Scientific and Practical Applications. *Science* **1996**, *271*, 43−48.

(2) Tanaka, M.; Sackmann, E. Polymer-Supported Membranes As Models of the Cell Surface. *Nature* **2005**, *437*, 656−663.

(3) Safinya, C. R.; Roux, D.; Smith, G. S.; Sinha, S. K.; Dimon, P.; Clark, N. A.; Bellocq, A. M. Steric Interactions in a Model Multimembrane System: A Synchrotron X-Ray Study. *Phys. Rev. Lett.* **1986**, *57*, 2718−2721.

(4) Daillant, J.; Bellet-Amalric, E.; Braslau, A.; Charitat, T.; Fragneto, G.; Graner, F.; Mora, S.; Rieutord, F.; Stidder, B. Structure and fluctuations of a single floating lipid bilayer. *Proc. Natl. Acad. Sci. U. S. A.* **2005**, *102*, 11639−11644.

(5) Groen, D.; Gooris, G. S.; Barlow, D. J.; Lawrence, M. J.; van Mechelen, J. B.; Demé, B.; Bouwstra, J. A. Disposition of Ceramide in Model Lipid Membranes Determined by Neutron Diffraction. *Biophys. J.* **2011**, *100*, 1481−1489.

(6) Jablin, M. S.; Dubey, M.; Zhernenkow, M.; Toomey, R.; Majewski, J. Influence of Lipid Membrane Rigidity on Properties of Supporting Polymer. *Biophys. J.* **2011**, *101*, 128−133.

(7) Miller, C. E.; Majewski, J.; Watkins, E. B.; Mulder, D. J.; Gog, T.; Kuhl, T. L. Probing the Local Order of Single Phospholipid Membranes Using Grazing Incidence X-Ray Diffraction. *Phys. Rev. Lett.* **2008**, *100*, 058103.

(8) Salditt, T. Thermal Fluctuations and Stability of Solid-Supported Lipid Membranes. *J. Phys.: Condens. Matter* **2005**, *17*, R287−R314.

(9) Schneck, E.; Papp-Szabo, E.; Quinn, B. E.; Konovalov, O. V.; Beveridge, T. J.; Pink, D. A.; Tanaka, M. Calcium Ions Induce Collapse of Charged O-Side Chains of Lipopolysaccharides from Pseudomonas Aeruginosa. *J. R. Soc. Interface* **2009**, *6*, S671.

(10) König, S.; Bayerl, T. M.; Coddens, G.; Richter, D.; Sackmann, E. Hydration Dependence of Chain Dynamics and Local Diffusion in L-Alpha-Dipalmitoylphosphatidylcholine Multilayers Studied by Incoherent Quasi-Elastic Neutron Scattering. *Biophys. J.* **1995**, *68*, 1871−1880.

(11) Rheinstädter, M. C.; Ollinger, C.; Fragneto, G.; Salditt, T. Collective Dynamics of Lipid Membranes Studied by Inelastic Neutron Scattering. *Phys. Rev. Lett.* **2004**, *93*, 108107.

(12) Jablin, M. S.; Zhernenkow, M.; Toperverg, B. P.; Dubey, M.; Smith, H. L.; Vidyasagar, A.; Toomey, R.; Hurd, A. J.; Majewski, J. In-Plane Correlations in a Polymer-Supported Lipid Membrane Measured by Off-Specular Neutron Scattering. *Phys. Rev. Lett.* **2011**, *106*, 138101.

(13) Schneck, E.; Demé, B.; Gege, C.; Tanaka, M. Membrane Adhesion via Homophilic Saccharide-Saccharide Interactions Investigated by Neutron Scattering. *Biophys. J.* **2011**, *100*, 2151.

(14) Schneck, E.; Rehfeldt, F.; Oliveira, R. G.; Gege, C.; Demé, B.; Tanaka, M. Modulation of Inter-Membrane Interaction and Bending Rigidity of Biomembrane Models via Carbohydrates Investigated by Specular and Off-Specular Neutron Scattering. *Phys. Rev. E* **2008**, *78*, 061924.

(15) Abuillan, W.; Vorobiew, A.; Hartel, A.; Jones, N. G.; Englstler, M.; Tanaka, M. Quantitative Determination of the Lateral Density and Intermolecuar Correlation between Proteins Anchored on the Membrane Surfaces Using Grazing Incidence Small-Angle X-ray Scattering and Grazing Incidence X-ray Fluorescence. *J. Chem. Phys.* **2012**, *137*, 204907.
(16) Leveiller, F.; Böhm, C.; Jacquemain, D.; Möhwald, H.; Leiserowitz, L.; Kjaer, K.; Als-Nielsen, J. Two-Dimensional Crystal Structure of Cadmium Arachidate Studied by Synchrotron X-Ray Diffraction and Reflectivity. *Langmuir* **1994**, *10*, 819−829.
(17) Müller-Buschbaum, P.; Cubitt, R.; Petry, W. Nanostructured Diblock Copolymer Films: A Grazing Incidence Small-Angle Neutron Scattering Study. *Langmuir* **2003**, *19*, 7778−7782.
(18) Liu, H.-J.; Jeng, U.-S.; Yamada, N. L.; Su, A.-C.; Wu, W.-R.; Su, C.-J.; Lin, S.-J.; Wei, K.-H.; Chiu, M.-Y. Surface and Interface Porosity of Polymer/Fullerene-Derivative Thin Films Revealed by Contrast Variation of Neutron and X-ray Reflectivity. *Soft Matter* **2011**, *7*, 9276−9282.
(19) Novikova, N. N.; Zheludeva, S. I.; Konovalov, O. V.; Kovalchuk, M. V.; Stepina, N. D.; Myagkov, I. V.; Godovsky, Y. K.; Makarova, N. N.; Tereschenko, E. Y.; Yanusova, L. G. Total Reflection X-ray Fluorescence Study of Langmuir Monolayers on Water Surface. *J. Appl. Crystallogr.* **2003**, *36*, 727−731.
(20) Yun, W. B.; Bloch, J. M. X-ray near Total External Fluorescence Method: Experiment and Analysis. *J. Appl. Phys.* **1990**, *68*, 1421−1428.
(21) Padmanabhan, V.; Daillant, J.; Belloni, L. Specific Ion Adsorption and Short-Range Interactions at the Air Aqueous Solution Interface. *Phys. Rev. Lett.* **2007**, *99*, 086105.
(22) Schneck, E.; Schubert, T.; Konovalov, O.; Quinn, B.; Gutsmann, T.; Brandenburg, K.; Oliveira, R. G.; Pink, D.; Tanaka, M. Quantitative Determination of Ion Distributions in Bacterial Lipopolysaccharide Membranes by Grazing-Incidence X-ray Fluorescence. *Proc. Natl. Acad. Sci. U. S. A.* **2010**, *107*, 9147−9151.
(23) Basu, J. K.; Boulliard, J. C.; Capelle, B.; Daillant, J.; Guenoun, P.; Mays, J. W.; Yang, J. Direct Probe of End-Segment Distribution in Tethered Polymer Chains. *Macromolecules* **2007**, *40*, 6333−6339.
(24) Fenter, P.; Cheng, L.; Rihs, S.; Machesky, M.; Bedzyk, M. J.; Sturchio, N. C. Electrical Double-Layer Structure at the Rutile-Water Interface as Observed in Situ with Small-Period X-Ray Standing Waves. *J. Colloid Interface Sci.* **2000**, *225*, 154−165.
(25) Schollmeyer, H.; Guenoun, P.; Daillant, J. Ion Distribution in Polyelectrolyte Multilayers with Standing-Wave X-ray Fluorescence. *J. Phys. Chem. B* **2007**, *111*, 4036−4042.
(26) Wang, J.; Caffrey, M.; Bedzyk, M. J.; Penner, T. L. Direct Profiling and Reversibility of Ion Distribution at a Charged Membrane/Aqueous Interface: An X-ray Standing Wave Study. *Langmuir* **2001**, *17*, 3671−3681.
(27) Nikitenko, Y. V. Neutron Standing Waves in Layered Systems: Formation, Detection, and Application in Neutron Physics and for Investigation of Nanostructures. *Phys. Part. Nuclei* **2009**, *40*, 890−947.
(28) Zhang, H.; Gallagher, P. D.; Satija, S. K.; Lindstrom, R. M.; Paul, R. L.; Russell, T. P.; Lambooy, P.; Kramer, E. J. Grazing Incidence Prompt Gamma Emissions and Resonance-Enhanced Neutron Standing Waves in a Thin Film. *Phys. Rev. Lett.* **1994**, *72*, 3044−3047.
(29) Grinyer, J.; Byun, S. H.; Chettle, D. R. In Vivo Prompt Gamma Neutron Activation Analysis of Cadmium in the Kidney and Liver. *Appl. Radiat. Isot.* **2005**, *63*, 475−479.
(30) Khokhlov, V. F.; Zaitsev, K. N.; Beliayev, V. N.; Kulakov, V. N.; Lipengolts, A. A.; Portnov, A. A. Prompt Gamma Neutron Activation Analysis of 10B and Gd in Biological Samples at the MEPhI Reactor. *Appl. Radiat. Isot.* **2009**, *67*, S251−S253.
(31) Marchal, D.; Bourdillon, C.; Demé, B. Small-Angle Neutron Scattering by Highly Oriented Hybrid Bilayer Membranes Confined in Anisotropic Porous Alumina. *Langmuir* **2001**, *17*, 8313−8320.
(32) Urizzi, P.; Souchard, J. P.; Nepveu, F. EDTA and DTPA Analogues of Dipalmitoylphosphatidylethanolamine as Lipophilic Chelating Agents for Metal Labeling of LDL. *Tetrahedron Lett.* **1996**, *37*, 4685−4688.
(33) Hillebrandt, H.; Tanaka, M. Electrochemical Characterization of Self-Assembled Alkoxysiloxane Monolayers on Indium Tin Oxide Semiconductor Electrodes. *J. Phys. Chem. B* **2001**, *105*, 4270.
(34) Koenig, B. W.; Strey, H. H.; Gawrisch, K. Membrane Lateral Compressibility Determined by NMR and X-ray Diffraction: Effect of Acyl Chain Polyunsaturation. *Biophys. J.* **1997**, *73*, 1954−1966.
(35) Parikh, A. N.; Beers, J. D.; Shreve, A. P.; Swanson, B. I. Infrared Spectroscopic Characterization of Lipid-Alkylsiloxane Hybrid Bilayer Membrane at Oxide Substrates. *Langmuir* **1999**, *15*, 5369−5381.
(36) Plant, A. Supported Hybrid Bilayer Membranes as Rugged Cell Membrane Mimics. *Langmuir* **1999**, *15*, 5128−5135.
(37) Alhaique, F.; Bertini, I.; Fragai, M.; Carafa, M.; Luchinat, C.; Parigi, G. Solvent ^{1}H NMRD Study of Biotinylated Paramagnetic Liposomes Containing Gd-bis-SDA-DTPA or Gd-DMPE-DTPA. *Inorg. Chim. Acta* **2002**, *331*, 151−157.
(38) Prosser, R. S.; Volkov, V. B.; Shiyanovskaya, I. V. Novel Chelate-Induced Magnetic Alignment of Biological Membranes. *Biophys. J.* **1998**, *75*, 2163−2169.
(39) ENSDF, Evaluated Nuclear Structure Data File (www.nndc.bnl.gov/ensdf).
(40) Zhang, H.; Satija, S. K.; Gallagher, P. D.; Dura, J. A.; Ritley, K.; Flynn, C. P.; Ankner, J. F. Grazing-Incidence Neutron Diffraction by Thin Films with Resonance Enhancement. *Phys. Rev. B* **1995**, *52*, 17502.
(41) Hubbell, J. H.; Seltzer, S. M. *Tables of X-Ray Mass Attenuation Coefficients and Mass Energy-Absorption Coefficients from 1 keV to 20 MeV for Elements Z = 1 to 92 and 48 Additional Substances of Dosimetric Interest*; National Institute of Standards and Technology: Gaithersburg, MD, 1995.
(42) Huang, Y.-S.; Jeng, U.-S.; Hsu, C.-H.; Torikai, N.; Lee, H.-Y.; Shin, K.; Hino, M. Complementary Neutron and X-ray Reflectivity for Structural Characterization of Porous Thin Films. *Physica B* **2006**, *385*−*386*, 667−669.
(43) Harms, A. A.; McCormack, G. Isotopic Conversion in Gadolinium-Exposure Neutron Imaging. *Nucl. Instrum. Methods* **1974**, *118*, 583−587.
(44) Harder, R.; Chaberek, S. The Interaction of Rare Earth Ions with Diethylenetriaminepentaacetic Acid. *J. Inorg. Nucl. Chem.* **1959**, *11*, 197−209.
(45) Gritmon, T. F.; Goedken, M. P.; Choppin, G. R. The Complexation of Lanthanides by Aminocarboxylate Ligands. *J. Inorg. Nucl. Chem.* **1977**, *39*, 2021.
(46) Wang, Z.; Ma, Y. Insights from Monte Carlo Simulations on Charge Inversion of Planar Electric Double Layers in Mixtures of Asymmetric Electrolytes. *J. Chem. Phys.* **2010**, *133*, 064704.
(47) Hu, K.; Bard, A. J. Use of Atomic Force Microscopy for the Study of Surface Acid-Base Properties of Carboxylic Acid-Terminated Self-Assembled Monolayers. *Langmuir* **1997**, *13*, 5114−5119.
(48) Qualmann, B.; Kessels, M. M.; Musiol, H.-J.; Sierralta, W. D.; Jungblut, P. W.; Moroder, L. Synthesis of Boron-Rich Lysine Dendrimers as Protein Labels in Electron Microscopy. *Angew. Chem., Int. Ed. Engl.* **1996**, *35*, 909−911.
(49) Gerelli, Y.; Porcar, L.; Fragneto, G. Lipid Rearrangement in DSPC/DMPC Bilayers: A Neutron Reflectometry Study. *Langmuir* **2012**, *28*, 15922−15928.
(50) Hemmerle, A.; Malaquin, L.; Charitat, T.; Lecuyer, S.; Fragneto, G.; Daillant, J. Controlling Interactions in Supported Bilayers from Weak Electrostatic Repulsion to High Osmotic Pressure. *Proc. Natl. Acad. Sci. U. S. A.* **2012**, *109*, 19938−19942.